Comparison of Polarization Mode Dispersion Emulators

Ivan T. Lima, Jr., *Student Member, IEEE, Member, OSA*, Reza Khosravani, *Member, IEEE*, Paniz Ebrahimi, Edem Ibragimov, *Member, IEEE*, Curtis R. Menyuk, *Fellow, IEEE, Fellow, OSA*, and Alan Eli Willner, *Senior Member, IEEE, Fellow, OSA*

***Abstract*—We analyze polarization mode dispersion (PMD) emulators comprised of a small number of sections of polarization-maintaining fibers with polarization scattering at the beginning of each section. Unlike previously studied devices, these emulators allow the emulation of a whole ensemble of fibers. We derive analytical expressions and determine two main criteria that characterize the quality of PMD emulation. The experimental results are in good agreement with the theoretical predictions.**

***Index Terms*—Optical fiber communication, optical polarization mode dispersion (PMD), polarization.**

I. Introduction

IT has been known for many years that all single-mode optical fibers are actually bimodal due to the presence of birefringence which breaks the two-fold degeneracy of the HE_{11} mode [1]. This effect is very weak in absolute terms—typically, $\Delta n/n \simeq 10^{-7}$. However, the wavelength of light is very small, $\lambda \simeq 1.5\ \mu$m, so that typical beat lengths are on the order of 3–30 m. This scale is very small compared to typical dispersive scale lengths, nonlinear scale lengths, and system scale lengths, all of which are typically hundreds or even thousands of kilometers. At the same time, the orientation of the axes of birefringence are changing over length scales of a fraction of a meter to a hundred meters, and beat lengths are typically tens of meters. Because the magnitude of an effect is inversely proportional to its scale length, the birefringence should be considered large but rapidly changing, relative to the system scale lengths of interest [2]. The length scale on which a single frequency changes its polarization state equals the length scale on which the orientation of the optical fiber birefringence changes, which is also the same order of magnitude as the beat length [3]; thus, the polarization state of the light is also rapidly changing. By contrast, the changes in the polarization states for all frequencies in a single wavelength channel are *nearly* identical, so that the polarization states in two different frequencies drift apart slowly if they start out the same. It is this differential drift that is the physical source of polarization mode dispersion (PMD).

The length scale on which this differential drift occurs varies over a wide range because it depends on the bandwidth of the signal channel as well as the properties of the optical fiber, but, in general, it is far longer than the length scale on which the polarization states of individual frequencies randomize on the Poincaré sphere [2]. Values range from tens of kilometers to tens of thousands of kilometers. The differential drift in the frequency domain leads to spreading in the time domain, reducing the power margin and increasing the bit error rate (BER). This effect becomes more important as the data rate of a single channel increases because the bandwidth of a single channel increases with the data rate. This effect must be overcome to implement 40-Gb/s transmission in single-wavelength channels over the current fiber plant in many systems, and, in some cases, it can be a seriously limiting factor in systems in which the single-channel rate is 10 Gb/s. Verifying that systems operate properly in the presence of large PMD is something that any system designer must do when marketing systems in which single channels operate at 10 Gb/s, 40 Gb/s, or higher [4], [5].

Because of the statistical nature of PMD, these verification experiments are hard to conduct. The axes of birefringence inside an optical fiber randomly change on a time scale that varies between milliseconds and hours, depending on the external conditions. The PMD and the polarization states in the fiber change on the same time scale. Ideally, one would like to know the outage probability for any system—the probability that, as the polarization parameters of the fiber randomly change, the power penalty due to PMD will fall outside an acceptable range. In order to determine that, one would like to observe the system's behavior as it passes through a large number of states. However, it is difficult in practice to carry out experiments in the field that are long enough in time to observe enough states to predict the outage probability. In the laboratory, the situation is even worse. Modern-day optical fiber has much lower PMD

Manuscript received March 20, 2001; revised August 20, 2001. This work was supported in part by the Air Force Office of Scientific Research, the Department of Energy, the National Science Foundation, the Defense Advanced Research Projects Agency Next Generation Internet, and the Charles Lee Powell Foundation.

I. T. Lima, Jr., is with the Department of Computer Science and Electrical Engineering, University of Maryland Baltimore County, Baltimore, MD 21250 USA (e-mail: lima@engr.umbc.edu).

R. Khosravani was with the University of Southern California, Los Angeles, CA 90089 USA. He is now with Phaethon Communications, Inc., Fremont, CA 94538-3140 USA (e-mail: reza@phaethoncommunications.com).

P. Ebrahimi is with the Department of Electrical Engineering–Systems, University of Southern California, Los Angeles, CA 90089-8729 USA (e-mail: pebrahim@usc.edu).

E. Ibragimov was with the University of Maryland Baltimore County, Baltimore, MD 21250 USA. He is now with Yafo Networks, Hanover, MD 21076 USA (e-mail: eibragimov@yafonet.com).

C. R. Menyuk is with the Laboratory for Telecommunication Sciences Adelphi, MD 20783-1197 USA, and with the Department of Computer Science and Electrical Engineering, University of Maryland Baltimore County, Baltimore, MD 21250 USA (e-mail: menyuk@umbc.edu).

A. E. Willner is with the Department of Electrical Engineering—Systems, University of Southern California, Los Angeles, CA 90089-8729 USA (e-mail: willner@usc.edu).

Publisher Item Identifier S 0733-8724(01)10206-9.

than does much of the current fiber plant in the ground. Values of today's commercial fiber are on the order of 0.1 ps/km$^{1/2}$ or less, while values of 1.0 ps/km$^{1/2}$ or even higher are not uncommon in fiber that is currently in the ground. Thus, even if it is possible to follow the behavior over long periods of time in the laboratory—and to use methods that are only possible in a laboratory to enhance the rate at which the fiber states change—it is nearly impossible to obtain high-PMD fiber in the first place.

Thus, there is a need for PMD emulators that have the same properties as high-PMD optical fibers but that, at the same time, can be rapidly scrolled through a large number of different configurations [6], [7] so that it is possible to accurately determine the outage probabilities. In the scientific literature today, it is not uncommon to see emulators that are built using three, two, or sometimes even just one section of high-birefringence fiber or some other high-birefringence material with either polarization rotators or scramblers at the ends or between the sections. There are also emulators that consist of as many as 15 sections of high-birefringence fibers that are directly spliced together. It is natural to ask to what extent these emulators mimic the behavior of real optical fiber transmission systems. What is required in order for an emulator to reliably model the behavior of a real optical fiber when testing a compensator or a wavelength division multiplexed (WDM) system? In this paper, we address this question, and we show that most of the emulators that are currently being used are inadequate. In particular, we find that approximately 10–15 sections with rotators or scramblers between them are required to model an optical fiber. Using fewer sections is insufficient, and it is insufficient for most applications to use an emulator in which the orientations of the axes of birefringence between the sections are fixed.

First, we must establish criteria for judging when an emulator is adequate. These criteria are, to some degree, arbitrary. We use two criteria.

1) For an emulator with a given PMD, the differential group delay (DGD) should be Maxwellian distributed at every frequency [8]. We demand that the actual distribution appear indistinguishable from a Maxwellian distribution when plotted on a linear scale. This convergence is quantified by the integral of the root mean square (rms) difference between the actual distribution and the ideal distribution.
2) For an emulator with a given PMD, the frequency autocorrelation function of the dispersion vector should tend quadratically toward zero as the frequency separation increases [9]. In practice, we demand that the autocorrelation background is lower than 10%.

A third criterion that we initially tried to apply is that for almost all choices of the parameters of the emulator, the DGD should be Maxwellian distributed as a function of frequency. This criterion turned out to be too stringent to be useful. Moreover, we verified that when criteria 1) and 2) hold, the second-order PMD has the expected hyperbolic-secant distribution [10], giving some indication that the first two criteria are sufficient to assure the expected behavior for the higher order PMD. Although these criteria are, to some extent, arbitrary, it will become readily apparent to the reader that they are minimal. The DGD distribution of a three-section emulator differs dramatically from a Maxwellian distribution and cuts off at a value close to the expected DGD so that the outage probability that it yields for a given PMD will be far lower than in real fibers.

The remainder of this paper is organized as follows. In Section II, we present the basic theory that allows us to determine the DGD distribution. In Section III, we discuss emulators with a fixed orientation between sections. In Section IV, we discuss emulators with a uniform scattering on the Poincaré sphere between sections. In Section V, we discuss emulators with rotators between the sections. We present our experimental results in this section. Section VI describes approaches for optimizing the emulator design. Finally, Section VII contains the conclusions.

II. Basic Theory

Here we revisit the two-step derivation of the concatenation rule of polarization dispersion vectors that is used as the basis for the development of the analytical theory of PMD emulators. This concatenation rule was first derived by Gisin and Pellaux [11].

The frequency-dependent evolution of the states of polarization in optical fibers can be described by the following vector equation:

$$\frac{d\mathbf{s}}{d\omega} = \mathbf{\Omega} \times \mathbf{s} \tag{1}$$

where $\mathbf{s}$ is the three-dimensional (3-D) Stokes vector and $\mathbf{\Omega}$ is the polarization dispersion vector [12]. The DGD $\Delta\tau$ between the two principal states of polarization can be expressed as the length of the vector $\mathbf{\Omega}$

$$\Delta\tau = |\mathbf{\Omega}| = \sqrt{\Omega_x^2 + \Omega_y^2 + \Omega_z^2}. \tag{2}$$

The polarization vector $\mathbf{s}_n$ of the light after n sections of polarization-maintaining fiber, and the initial polarization vector $\mathbf{s}_i$, are related by the equation $\mathbf{s}_n = \mathsf{T}\mathbf{s}_i$, where T is the 3×3 Müller transmission matrix. Here, we assume that all of the frequency components of the signal are launched with the same initial Stokes vector $\mathbf{s}_i$. Let B be the rotation matrix that transforms the Stokes vector from the input of the $(n+1)$-th polarization-maintaining fiber section to the output of the $(n+m)$-th section, so that $\mathbf{s}_{n+m} = \mathsf{B}\mathbf{s}_n$. Using these relations, we may write

$$\frac{d\mathbf{s}_n}{d\omega} = \mathsf{T}'\mathbf{s}_i = \mathsf{T}'\mathsf{T}^{-1}\mathbf{s}_n, \tag{3}$$

and

$$\frac{d\mathbf{s}_{n+m}}{d\omega} = \mathsf{B}'\mathbf{s}_n + \mathsf{B}\frac{d\mathbf{s}_n}{d\omega} = [\mathsf{B}'\mathsf{B}^{-1} + \mathsf{B}\mathsf{T}'\mathsf{T}^{-1}\mathsf{B}^{-1}]\mathbf{s}_{n+m} \tag{4}$$

where the prime indicates a derivative with respect to ω. Comparing (3) and (4) to (1), the formula that relates the polarization dispersion vector after the nth section to the polarization dispersion vector after the $(n+m)$-th section may be written as

$$\mathbf{\Omega}_{n+m} = \Delta\mathbf{\Omega} + \mathsf{B}\mathbf{\Omega}_n \tag{5}$$

where $\mathbf{\Omega}_n$ is the polarization dispersion vector of the first n sections and $\Delta\mathbf{\Omega}$ is the polarization dispersion vector of the next

m sections. Explicitly, the quantities $\Delta\mathbf{\Omega}$ and $\mathsf{B}'\mathsf{B}^{-1}$ are related by

$$\mathsf{B}'\mathsf{B}^{-1} = \begin{pmatrix} 0 & -\Delta\Omega_z & \Delta\Omega_y \\ \Delta\Omega_z & 0 & -\Delta\Omega_x \\ -\Delta\Omega_y & \Delta\Omega_x & 0 \end{pmatrix}. \tag{6}$$

The identity $\mathsf{B}[\mathbf{\Omega}_n \times (\mathsf{B}^{-1}\mathbf{s}_{n+m})] = (\mathsf{B}\mathbf{\Omega}_n) \times \mathbf{s}_{n+m}$ represents a basis transformation caused by the propagation through the last m sections.

A practical way to obtain the polarization dispersion vector of a concatenation of polarization-maintaining fibers is to solve (5) recursively by choosing $m = 1$. Let $\mathbf{\Omega}_n$ and $\Delta\mathbf{\Omega}_{n+1}$ be the polarization dispersion vectors of the first n sections and the $(n+1)$-th section, respectively. Then, we may write the following recursion formula for the total DGD:

$$\Delta\tau_{n+1}^2 = |\Delta\mathbf{\Omega}_{n+1}|^2 + |\mathsf{B}\mathbf{\Omega}_n|^2 + 2|\Delta\mathbf{\Omega}_{n+1}||\mathsf{B}\mathbf{\Omega}_n|\cos(\theta_{n+1}) \tag{7}$$

where θ_{n+1} is the angle between $\Delta\mathbf{\Omega}_{n+1}$ and $\mathsf{B}\mathbf{\Omega}_n$. The rms DGD $\langle\Delta\tau^2\rangle^{1/2}$ of an ensemble of PMD sources, all with the same respective values of $|\Delta\Omega_i|$ but with randomly chosen orientations in the 3-D space, is given by

$$\langle\Delta\tau^2\rangle^{1/2} = \left[\sum_{i=1}^{N} |\Delta\Omega_i|^2\right]^{1/2} \tag{8}$$

as in [13], provided that the transmission matrices T_i that characterize the polarization dispersion vectors are obtained from a distribution such that $\langle\cos(\theta_i)\rangle = 0$. Because the probability density function of the DGD (for large n) is Maxwellian, the mean DGD can be obtained from the rms DGD, as in [14]

$$\langle\Delta\tau\rangle = \left[\frac{8}{3\pi}\langle\Delta\tau^2\rangle\right]^{1/2}. \tag{9}$$

III. PMD Emulators With Fixed Orientations

PMD emulators consisting of several sections of polarization-maintaining fiber with unequal lengths whose orientations are fixed [15] have recently been used to test polarization analyzers and for the comparison of different PMD measurement devices and techniques [16]. As long as the wavelength of light is short, compared to the beat length in the fiber (which is, in turn, short compared to the correlation length of the fiber, as is the case in polarization-maintaining fiber), it is legitimate to assume that the polarization state of the light circles the local polarization eigenstate on the Poincaré sphere on a length scale equal to half the beat length [3]. In any polarization-maintaining fiber, there is some random coupling between the polarizations due to the finite ratio between the beat length and the autocorrelation length [17], but it is negligible in our system.

The propagation matrix of a section of polarization-maintaining fiber whose axes of birefringence are rotated at the beginning of the section through an angle θ while keeping the angle fixed at the section's end can be described by the matrix equation

$$\mathsf{B} = \mathsf{R}_x\mathsf{R}_z^{-1} \tag{10}$$

where the matrix R_z accounts for the initial rotation while the matrix R_x accounts for the propagation through the fiber section. The matrix R_z is given by

$$\mathsf{R}_z = \begin{pmatrix} \cos 2\theta & -\sin 2\theta & 0 \\ \sin 2\theta & \cos 2\theta & 0 \\ 0 & 0 & 1 \end{pmatrix}. \tag{11}$$

The matrix R_x is given by

$$\mathsf{R}_x = \begin{pmatrix} 1 & 0 & 0 \\ 0 & \cos 2\phi & -\sin 2\phi \\ 0 & \sin 2\phi & \cos 2\phi \end{pmatrix} \tag{12}$$

where

$$\phi = bL_n + b'L_n\omega \tag{13}$$

$2b = \beta_1 - \beta_2$ is the difference between the wavenumbers of the fast and the slow fiber axes, which is a consequence of the birefringence $b' = db/d\omega$, and L_n is the length of the n-th segment.

From (6) and (10), we obtain

$$\Delta\mathbf{\Omega}_n = \begin{pmatrix} 2b'L_n \\ 0 \\ 0 \end{pmatrix}. \tag{14}$$

Using (5) and (14), we obtain the following recursive relation for the polarization dispersion vector:

$$\begin{pmatrix} \Omega_{x_n} \\ \Omega_{y_n} \\ \Omega_{z_n} \end{pmatrix} = \begin{pmatrix} 2b'L_{n+1} \\ 0 \\ 0 \end{pmatrix} + \begin{pmatrix} 0 & 1 & 0 \\ -\cos 2\phi & 0 & -\sin 2\phi \\ -\sin 2\phi & 0 & \cos 2\phi \end{pmatrix} \begin{pmatrix} \Omega_{x_{n-1}} \\ \Omega_{y_{n-1}} \\ \Omega_{z_{n-1}} \end{pmatrix} \tag{15}$$

when the axes of birefringence of consecutive sections consistently rotate by $\theta = \pi/4$ either clockwise or counterclockwise. In this configuration, the signal that propagates through the fast axis in one section always splits into equal parts that propagate along the fast and slow axes of the following section. Likewise, the signal that propagates on the slow axis splits into two equal parts in the following section. This configuration leads to a rapid frequency decorrelation of the resultant polarization dispersion vector as the number of sections increases. By contrast, splices with angles close to 0 and $\pi/2$ yield a very slow frequency decorrelation as the number of fiber sections increases.

With as few as 15 sections of polarization-maintaining fiber spliced at $\theta = \pi/4$, with unequal lengths chosen randomly, as described in detail in Section VI, we show in Fig. 1 that the probability density function (pdf) of the DGD for an ensemble of frequencies is well described by a Maxwellian distribution. We verified that this behavior is typical for different random choices of the section lengths. Because the correlation bandwidth of the polarization dispersion vector in Fig. 1 is of the order of $0.5/\langle\Delta\tau\rangle = 10.4$ GHz [8], we expect to find no more than 400 uncorrelated samples in the 4-THz frequency range.

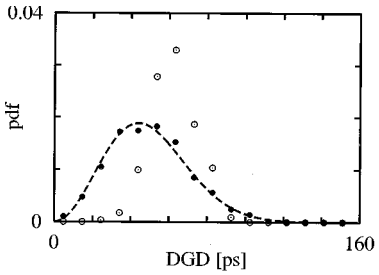

Fig. 1. The density function of the DGD of an ensemble of frequencies, normalized by the expected value of the DGD. We consider here a fixed emulator with 15 sections. The frequency bandwidth is 4 THz. Open circles indicate the density function of a fixed emulator with fiber sections spliced at $\theta = \pi/4$. Solid circles are the density function of an emulator with the same section lengths, but spliced at randomly chosen angles. The dashed line represents the Maxwellian fit to the expected value of the DGD, that is, equal to 48 ps, according to (9).

We also show, in Fig. 1, a typical pdf of the DGD for an emulator with the same 15 polarization-maintaining fiber sections but spliced at random angles. The emulator with randomly chosen splicing angles is likely to have either undesirable cancellation of the polarization dispersion vectors between consecutive sections when these angles are close to $\pi/2$ or to behave like a long piece of polarization-maintaining fiber when the sections are nearly aligned.

We have shown that it is possible to optimize PMD emulators with fixed sections to obtain a DGD distribution in good agreement with a Maxwellian distribution over an ensemble of frequencies. However, the practical use of such emulators to study PMD impairments in communications systems is limited due to the wide frequency range that one needs to sweep in order to obtain good statistics. One must assume that the behavior of the fiber and the optical sources remains the same at all frequencies even when studying only a single channel—something that is not typically the case in real communications systems. Although one might use temperature and other environmental variations to obtain additional statistical variations beyond what is possible by varying the frequency, one cannot obtain a rapidly changing and reproducible emulator using this approach. Finally, it is not possible to study WDM systems using an emulator with fixed sections. In WDM systems, the frequency dependence of the dispersion map, the gain and the loss, and system components play a big role in the system performance. Thus, even if it were possible to vary the frequency of the laser sources while keeping their spacing fixed—a very difficult experiment, indeed—one would still not reproduce the correct system behavior of an ensemble of different fiber realizations. In practice, one can only vary the ambient environment of the emulator, which is slow and irreproducible.

IV. PMD Emulators With Uniform Scattering Between Sections

In this section, we analyze PMD emulators that consist of sections of polarization-maintaining fiber with polarization scramblers at the beginning of each section. The polarization scramblers uniformly scatter the polarization state over the Poincaré sphere and can be made using polarization controllers. Because the polarization dispersion vector is uniformly scattered over the Poincaré sphere, the random variable $\cos\theta$ in (7) is uniformly distributed between -1 and 1. Equation (7) allows us to iteratively obtain analytical expressions for the pdf of the DGD of emulators with an arbitrary number of sections. We show in the Appendix that the recursion formula for the pdf is

$$f_{\Delta\tau_{n+1}} = \frac{\Delta\tau_{n+1}}{2a} \int_{|\Delta\tau_{n+1}-a|}^{\Delta\tau_{n+1}+a} \frac{f_{\Delta\tau_n}}{\Delta\tau_n}\, d\Delta\tau_n \tag{16}$$

where $\Delta\tau_{n+1}$ is the total DGD of all $n+1$ sections and a is the DGD of the $(n+1)$-th section, which is assumed to be known. To start the recursion relation, we note that with one section

$$f_{\Delta\tau_1} = \delta(\Delta\tau_1 - a) \tag{17}$$

where $\delta(\cdot)$ is the Dirac delta function. Assuming that the DGD is the same for all sections, we then obtain for three sections

$$f_{\Delta\tau_3} = \frac{\Delta\tau_3}{4a^3} \begin{cases} 2\Delta\tau_3, & 0 \le \Delta\tau_3 \le a \\ 3a - \Delta\tau_3, & a < \Delta\tau_3 \le 3a \\ 0, & \text{otherwise} \end{cases} \tag{18}$$

and for five sections, as shown in (19) at the bottom of the page.

Equation (16) rapidly converges to a Maxwellian distribution. Plots of the distribution functions of emulators with three, five, and 10 sections are compared to Maxwellian distributions in Figs. 2, 3, and 4, respectively. With three sections, the pdf differs significantly from a Maxwellian distribution when the DGD is large. With five sections, the shape of the pdf is substantially closer to Maxwellian, and for 10 sections, the pdf of the DGD is already almost indistinguishable from a Maxwellian distribution on a linear scale.

Results similar to those presented in this section have been presented by Djupsjöbacka [18] and Karlsson [19] in the case of emulators with equal length sections.

$$f_{\Delta\tau_5} = \frac{\Delta\tau_5}{96a^5} \begin{cases} 6\left(5a^2\Delta\tau_5 - \Delta\tau_5^3\right), & 0 \le \Delta\tau_5 \le a \\ -10a^3 + 60a^2\Delta\tau_5 - 30a\Delta\tau_5^2 + 4\Delta\tau_5^3, & a < \Delta\tau_5 \le 3a \\ 125a^3 - 75a^2\Delta\tau_5 + 15a\Delta\tau_5^2 - \Delta\tau_5^3, & 3a < \Delta\tau_5 \le 5a \\ 0, & \text{otherwise.} \end{cases} \tag{19}$$

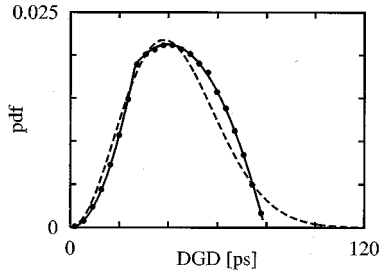

Fig. 2. Distribution function of the DGD for an emulator with three sections and uniform polarization scattering over the Poincaré sphere at the beginning of each section. The mean DGD of this emulator is 42 ps. Open circles are results of Monte Carlo simulations. The solid line represents the analytical pdf from (18). The dashed line represents the Maxwellian fit. The Monte Carlo simulations in this figure and succeeding figures used 10^5 realizations.

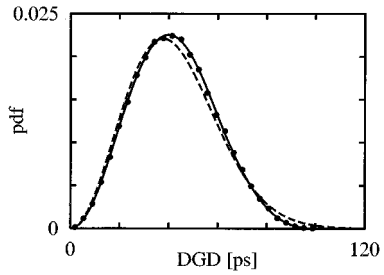

Fig. 3. Distribution function of the DGD for an emulator with five sections and uniform polarization scattering over the Poincaré sphere at the beginning of each section. The mean DGD of this emulator is 42 ps. Open circles are results of Monte Carlo simulations. The solid line represents the analytical pdf from (18). The dashed line represents the Maxwellian fit.

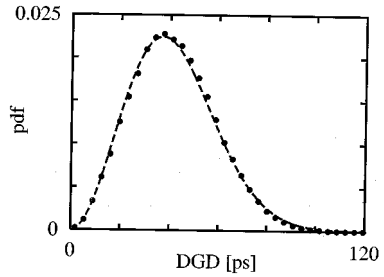

Fig. 4. Distribution function of the DGD for an emulator with ten sections and uniform polarization scattering over the Poincaré sphere at the beginning of each section. The mean DGD of this emulator is 42 ps. Open circles show the results of Monte Carlo simulations. The dashed line represents the Maxwellian fit.

V. PMD Emulators With Rotatable Sections

A. Theory

In this section, we study PMD emulators that are made of randomly rotated sections of polarization-maintaining fiber. In this case, the matrix B defined in Section II becomes

$$\mathsf{B} = \mathsf{R}_z \mathsf{R}_x \mathsf{R}_z^{-1} \tag{20}$$

where R_z and R_x are defined in (11) and (12). Using (11), (12), and (20), we then obtain

$$\mathsf{B}'\mathsf{B}^{-1} = 2b' L_n \begin{pmatrix} 0 & 0 & \sin 2\theta \\ 0 & 0 & -\cos 2\theta \\ -\sin 2\theta & \cos 2\theta & 0 \end{pmatrix} \tag{21}$$

which, using (6), implies

$$\begin{aligned} \Delta\Omega_x &= 2b' L_n \cos 2\theta \\ \Delta\Omega_y &= 2b' L_n \sin 2\theta \\ \Delta\Omega_z &= 0. \end{aligned} \tag{22}$$

This result implies that the polarization dispersion vector of each section of polarization-maintaining fiber lies in the XY plane and the direction of $\Delta\boldsymbol{\Omega}$ depends on the angle θ between the axes of birefringence of the fiber and the X axis of the fixed reference frame. The length of $\Delta\boldsymbol{\Omega}$ is proportional to $2b'$, the linear birefringence, multiplied by the length of the fiber section L_n.

There is a subtle point of which the reader should be aware when studying emulators with rotatable sections. In many theoretical studies, it is possible to remove the rotation of the carrier frequency from the definition of ϕ in (13); however, that is not the case here. The rotation due to a nonzero ϕ is entirely responsible for lifting the polarization dispersion vector out of the XY plane on the Poincaré sphere. If we do not take this rotation into account, we find, theoretically, that the pdf at the carrier frequency becomes approximately Rayleigh distributed, in contrast to real fibers for which it is Maxwellian distributed. Along these lines, we also note that a potential difficulty with emulators that consist of rotatable equal-length sections with a fixed birefringence is that all the frequency-dependent characteristics repeat periodically in frequency. Thus, at certain periodically spaced frequencies ϕ becomes a multiple of π and at those frequencies the pdf becomes Rayleigh distributed. Moreover, the autocorrelation function becomes periodic. This phenomenon, which does not occur in real fibers, can be avoided in practice by using sections of variable length when constructing emulators. In older computational studies of PMD, it was often the practice to use equal-length sections of fiber with random rotations between the sections. In principle, this approach is subject to an unrealistic frequency periodicity just like physical emulators with equal-length sections. In practice, this effect can be avoided by taking sufficiently small steps, but this obsolete numerical practice is always less efficient than the coarse step method that uses scramblers between the sections [17].

We show in the Appendix that it is possible to obtain an analytical expression for the pdf of the DGD in emulators in which the sections are rotated, just as it is possible to obtain analytical expressions when the polarization is uniformly scattered between the sections. However, in this case, the expressions are considerably more complex, and the complexity increases rapidly with the number of sections. The expression for three sections with a constant DGD in each section may be written in integral form as

$$\begin{aligned} f_{\Delta\tau_3} &= \frac{2\Delta\tau_3}{a\pi^2} \int_{\mathcal{F}} [(4a^2 - v^2) G(v)]^{-1/2}\, dv \\ G(v) &= 1 - \sin^2(2\phi) \left(1 - \frac{v^2}{4a^2}\right) - \frac{\left(\Delta\tau_3^2 - v^2 - a^2\right)}{4a^2} \end{aligned} \tag{23}$$

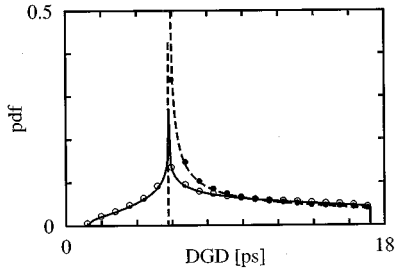

Fig. 5. Distribution function of the DGD for an emulator with three rotated sections. The rotation angles have a uniform pdf between 0 and 2π. Open circles represent Monte Carlo simulations and solid line represents the analytical pdf for $\lambda = 1.551\ \mu$m. Solid circles represent Monte Carlo simulations and the dashed line represents the analytical pdf for $\lambda = 1.552\ \mu$m. The mean DGD of this emulator is 9.1 ps at 1.551 μm and 9.4 ps at 1.552 μm.

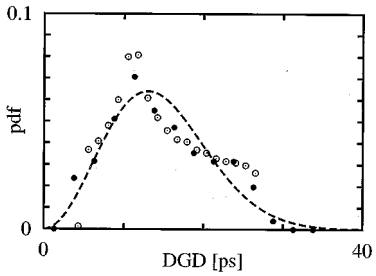

Fig. 6. Distribution function of the DGD for an emulator with three sections and rotatable fiber couplers rotated uniformly by angles between 0 and 2π. Monte Carlo simulations and experimental results are included for $\lambda = 1.55\ \mu$m. The lengths of the polarization-maintaining fiber sections are 5.14, 6.81, and 4.67 m. The mean DGD of this emulator is 17 ps. Open circles are the results of Monte Carlo simulations. Solid circles are experimental results. The dashed line represents the Maxwellian fit.

where we recall that ϕ is defined in (13) and a is the DGD per section. The range of integration is given by

$$\mathcal{F} = \left\{ v \in (0, 2a) \left| \frac{\left(\Delta\tau_3^2 - v^2 - a^2\right)^2}{\left[1 - \sin^2(2\phi)\left(1 - \frac{v^2}{4a^2}\right)\right]} < 4a^2 \right. \right\}. \tag{24}$$

Equation (23) can be integrated analytically, but the expression is complicated, and we do not include it here. The complexity of this case relative to the case of uniform scattering is due to the nonuniform scattering on the Poincaré sphere provided by the rotators. Each rotatable section only scatters the X and Y components of the polarization. The nonuniform scattering over the Poincaré sphere is also responsible for the implicit frequency dependence of the pdf that stems from the presence of ϕ in (23). We show numerical and analytical pdfs in Fig. 5 for two frequencies 1-nm apart. From Fig. 5, we conclude that this three-section emulator cannot reproduce a value for the DGD smaller than 62% of the expected DGD at 1.552 μm.

B. Experiments

We experimentally studied PMD emulators with independently rotatable connectors placed at the beginning of each section of polarization-maintaining fiber. The transmission matrix in each section of this configuration is given by (10). This transmission matrix is the same as the one given in (20), with rotatable sections, to within a frequency-independent unitary operation at the output. Hence, they are statistically equivalent.

In the experiments, we have used sections of polarization-maintaining fiber (Fiber Core, HiBi, Bow-Tie) connected by rotatable key fiber-channel connectors, the fiber-optic connector standard by NTT and NEC. We began our experimental studies by investigating a three-section emulator in which we randomly rotated the connectors, uniformly from 0 to 2π, to emulate different realizations. We measured the DGD values using the Jones matrix method. Fig. 6 shows that a three-section polarization-maintaining fiber emulator cannot mimic the DGD distribution of a real optical fiber span, as predicted by theory.

We then increased the number of sections in the experiment to 15, which is the minimum number of sections that theory indicates should yield good agreement with a real optical fiber. The beat length of the polarization-maintaining fibers approximately equals 1.2 mm at 633 nm, and the average length of the sections approximately equals 7 m. Explicitly, we chose the lengths of the fifteen sections to equal 5.1, 6.8, 8.6, 7.4, 6.3, 6.7, 10.0, 8.6, 5.4, 7.2, 6.9, 7.1, 6.1, 7.4, and 4.6, for which the standard deviation is equal to 20% of the mean length. As we will discuss in more detail in the next section, this choice of the standard deviation provides a good balance between avoiding the problems that occur with constant-length sections while allowing the total DGD to vary widely. The total loss of this emulator is between 6 dB and 10 dB, depending on the rotation angles of the polarization-maintaining fiber sections. The polarization dependent loss has been measured to be less than 0.2 dB. Different realizations were again obtained by randomly rotating the connectors. The pdf for the emulator with 15 sections is shown in Fig. 7. A good agreement with a Maxwellian distribution was observed in accord with the theoretical prediction.

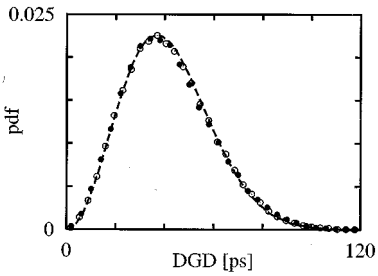

Fig. 7. Distribution function of the DGD for an emulator with 15 randomly rotatable sections. The mean DGD of this emulator is 42.6 ps. Open circles are results of Monte Carlo simulations. Solid circles are experimental results. The dashed line represents the Maxwellian fit.

In Fig. 8, we show both theoretical and experimental normalized autocorrelation functions of the polarization dispersion vector $\langle \mathbf{\Omega}(\omega) \cdot \mathbf{\Omega}(\omega_0)\rangle / \langle \mathbf{\Omega}(\omega_0) \cdot \mathbf{\Omega}(\omega_0)\rangle$ for the 15-section emulator. Good agreement between theory and experiment was again observed. In the theoretical work, we used 10 000 realizations. In the experimental work, we used 1000 realizations. In Fig. 8, we also show the theoretical autocorrelation functions for three-section and 100-section emulators with the same expected DGD. As in the case of the 15-section emulator, we used 10 000 fiber realizations. The section lengths are unequal but are the same in each realization. We chose the section length randomly using the algorithm described in Section VI. We verified that the results presented here are typical by studying many choices of the random lengths, as discussed in Section VI. A background autocorrelation level of 9.3% was observed for the 15-section emulator that decreases to 2.2% for the 100-section emulator. The

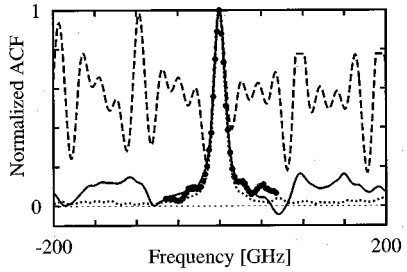

Fig. 8. Normalized autocorrelation function of the polarization dispersion vector of various PMD emulators with rotatable stages randomly rotated at the beginning of each section. The mean DGD of these emulators is 43 ps. Solid circles are experimental results with 15 sections. The dashed, solid, and dotted curves are, respectively, the results from simulations with three, 15, and 100 sections. The central wavelength is 1.55 μm.

background autocorrelation level is defined as the average value of the autocorrelation function, normalized to zero frequency separation for polarization dispersion vectors that are separated from each other by a frequency larger than the correlation bandwidth $\Delta f_c \approx 0.5/\langle\Delta\tau\rangle$ [8]. This background is vanishingly small for real optical-fiber spans, which are many times larger than the fiber correlation length, but it does not vanish for emulators for which the number of sections is typically small. At any frequency, there is a tendency of $\mathbf{\Omega}(\omega)$ to be positively correlated with $\mathbf{\Omega}(\omega_0)$. With one section, the normalized autocorrelation function always equals one. With two sections, we find that $\langle\mathbf{\Omega}(\omega)\cdot\mathbf{\Omega}(\omega_0)\rangle = \Delta\tau_2^2 + \Delta\tau_1^2/2\{1+\cos[\Delta\tau_2(\omega-\omega_0)]\}$, which is always positive, where $\Delta\tau_1$ and $\Delta\tau_2$ are, respectively, the DGDs of the first and second sections. As the number of sections increases, it becomes possible for the autocorrelation function to become negative, but it is not likely. Experiments using PMD emulators with a high background autocorrelation level will produce unreliable results due to high correlation of the polarization dispersion vector within the bandwidth of the optical signal. By any measure, the three-section emulator produces a background autocorrelation level that is unacceptably high.

VI. Emulator Design

In order to optimize the lengths and the number of sections in a controllable PMD emulator, we have defined two criteria that an emulator should satisfy.

1) *At each frequency, the pdf of the DGD should be Maxwellian distributed.* To quantify this property, we first normalize the expected DGD for the given PMD to 1 and write the corresponding Maxwellian pdf as $f_M(x)$. At each frequency f_i, the probability that the normalized DGD is in the range (x_{j-1}, x_j) is designated $P_{f_i}\{x_i \in (x_{j-1}, x_j)\}$. We then define the parameters

$$\sigma_d^2 = \frac{1}{N_f}\sum_{i=1}^{N_f}\sum_{j=1}^{N_b}\left|P_{f_i}\{x_i\in(x_j,x_{j-1})\} - \int_{x_{j-1}}^{x_j} f_M(x)\,dx\right|^2$$

$$\sigma_m^2 = \frac{1}{N_f}\sum_{i=1}^{N_f}|\langle x_{f_i}\rangle - 1|^2 \qquad (25)$$

where N_b is the number of bins and N_f is the number of frequencies. Physically, σ_d measures the mean square deviation of the pdf from a Maxwellian distribution while σ_m measures the spread of the mean normalized DGD of each frequency about the expected value of 1.

2) The background autocorrelation level should be close to zero. To characterize this property, we use the normalized background autocorrelation function

$$\mathrm{ACF}_B = \frac{1}{N_f}\sum_{|\omega_i-\omega_0|>\pi/\langle\Delta\tau\rangle}\left|\frac{\langle\mathbf{\Omega}(\omega_i)\cdot\mathbf{\Omega}(\omega_0)\rangle}{\langle\mathbf{\Omega}(\omega_0)\cdot\mathbf{\Omega}(\omega_0)\rangle}\right| \qquad (26)$$

where ω_i are N_f angular frequencies equally spaced outside the bandwidth of high correlation centered at ω_0.

We have investigated and attempted to optimize a variety of emulator designs. In two designs that we refer to as E1 and E2, we subdivide the total length of the emulator into some number of sections N, and we randomly vary this length using a uniform distribution up to twice the mean length. In design E1, we assume that the sections can be randomly rotated with respect to each other, and in design E2, we assume that there are polarization scramblers between each section so that the polarization state is uniformly scattered on the Poincaré sphere. In two other closely related designs, called EC1 and EC2, we assumed that each of the sections was cut in two parts and then spliced together at a fixed angle of 45°. This design substantially reduces the autocorrelation background at the cost of substantially increasing σ_d and σ_m. In EC1, the sections are rotated with respect to each other, and in EC2, there are scramblers between each section. In the final design that we considered, referred to as ED1, the sections decrease in length rather than being chosen randomly according to the formula $L_{i+1} = \alpha L_i$. We have found that choosing $\alpha = 0.85$ yields the best results, but, even in the best case, there is a tradeoff between minimizing σ_d and σ_m and reducing the background autocorrelation level.

When optimizing our designs, we examined 5000 cases. We used the following algorithm. For a fiber of length L_{tot} with N sections, the boundary between the k-th and the $(k+1)$-th section is located at distance kL_{tot}/N from the beginning of the fiber if the fiber has equal-length sections. We vary the actual location of this boundary randomly using a uniform random number generator in the range $[(2k-1)L_{\mathrm{tot}}/2N, [(2k+1)L_{\mathrm{tot}}/2N]$, for every k. For the design E1 with $N = 15$, corresponding to our experimental design, all of the best cases had a standard deviation of the section length between 20% and 45% of the mean length.

In addition to the two criteria stated at the beginning of the section, we attempted, at first, to apply a criterion in which we demanded that the vast majority of fiber realizations should yield a Maxwellian distribution of the DGDs at different frequencies. There were two problems with this criterion. First, there are many realizations, like the one in which all the orientations are lined up, in which the pdf of the DGD is not Maxwellian no matter how large the bandwidth is. Even with as many as 15 sections, the volume of the phase space of these realizations is large enough to substantially affect the overall result. Second, even with the realizations that have a

TABLE I

COMPARISON AMONG DIFFERENT PMD EMULATORS COMPRISED OF BIREFRINGENT SECTIONS. E1: EMULATORS WITH ROTATORS. E2: EMULATORS WITH POLARIZATION CONTROLLERS. EC1 AND EC2 : EMULATORS COMPRISED OF POLARIZATION ROTATORS AND POLARIZATION CONTROLLERS, RESPECTIVELY, WHOSE SECTIONS ARE COMPRISED OF TWO BIREFRINGENT FIBERS SPLICED AT $\pi/4$. ED1: EMULATOR WITH GEOMETRICALLY DECREASING LENGTHS WITH COEFFICIENT α. SUBSCRIPT r INDICATES QUANTITY IS AN AVERAGE OVER AN ENSEMBLE OF REALIZATIONS AT SINGLE FREQUENCY. SUBSCRIPT f INDICATES QUANTITY IS AN AVERAGE OVER AN ENSEMBLE OF FREQUENCIES WITH FIXED REALIZATION

Type	Sections	$\sigma^2_{\rm dr}$	$\sigma^2_{\rm mr}$	$\sigma^2_{\rm df}$	$\sigma^2_{\rm mf}$	ACF_B
E1	7 Optimized	6.81×10^{-4}	1.04×10^{-5}	4.05×10^{-1}	7.41×10^{-2}	31.36%
E1	10 Optimized	1.75×10^{-4}	7.53×10^{-6}	1.11×10^{-1}	7.23×10^{-2}	20.13%
E1	15 Random	6.07×10^{-5}	5.47×10^{-6}	6.51×10^{-2}	5.11×10^{-2}	9.38%
E1	15 Optimized	5.56×10^{-5}	5.53×10^{-6}	4.66×10^{-2}	5.63×10^{-2}	11.54%
E1	100 Random	4.71×10^{-5}	3.13×10^{-6}	1.15×10^{-3}	1.03×10^{-2}	2.19%
E2	15 Optimized	3.08×10^{-4}	1.87×10^{-5}	1.64×10^{-2}	3.22×10^{-2}	10.47%
EC1	15 Optimized	1.13×10^{-3}	4.82×10^{-3}	1.62×10^{-3}	4.85×10^{-3}	6.18%
EC2	15 Optimized	2.23×10^{-4}	1.61×10^{-5}	1.58×10^{-3}	3.90×10^{-3}	4.29%
ED1	15 $\alpha=0.85$	2.43×10^{-4}	1.20×10^{-5}	1.83×10^{-1}	7.59×10^{-2}	1.92%

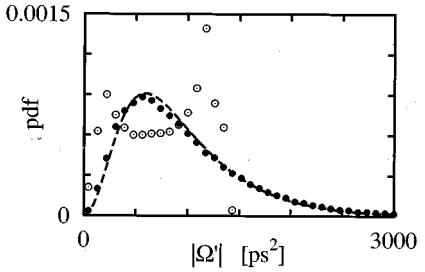

Fig. 9. Distribution function of the length of the second-order component of the polarization dispersion vector $\mathbf{\Omega}'$ for emulators with 15 and three polarization-maintaining fiber sections with rotatable stages randomly rotated at the beginning of each section. Both emulators have mean DGD of 44 ps. Open circles and solid circles are, respectively, the results from simulations with three and 15 sections. The dashed line represents the analytical fit.

Maxwellian distribution of the DGD, the bandwidth has to be unrealistically large, as discussed in Section III. We did, however, verify that the two criteria that we have chosen are sufficient to assure that the second-order PMD has the appropriate distribution. In Fig. 9, we show the distribution of the length of the polarization dispersion vector $\mathbf{\Omega}' = d\mathbf{\Omega}/d\omega$ with three and with 15 sections. In both cases, we used the procedure to optimize the lengths that we described at the beginning of this section. In a real fiber, the theoretically predicted pdf is [8]

$$f_{\Delta\tau} = \sqrt{\frac{2}{\pi}}\frac{\Delta\tau^2}{\alpha^3}\exp\left(\frac{\Delta\tau^2}{2\alpha^2}\right) \tag{27}$$

where $\alpha = \langle\Delta\tau\rangle(\pi/8)^{1/2}$. It is apparent that three sections are insufficient to obtain the correct pdf, but 15 sections yield a pdf that is almost indistinguishable from the analytical result on a linear scale.

We summarize the key results from our emulator design studies in Table I. We first note that even with just seven sections, the optimization procedure yields a reasonable Maxwellian distribution for design E1, although the background autocorrelation level remains high. With this number of sections, it is important to apply the optimization procedure to get a good result. By contrast, with 15 sections, we find that the difference the optimized σ_d^2 and one that came from a single random choice that corresponded to our experimental setup was only about 10%. Moreover, the values for σ_m^2 and the background autocorrelation level were actually somewhat *worse* for the optimized case. We observed that the design E2 converges more slowly to a Maxwellian pdf than does the design E1, even though it handles the randomization of the fields on the Poincaré sphere more rapidly. The reason is that the design E1 splits the power somewhat more effectively than does E2 among the different orientations. The splices at 45° in the composite sections in designs EC1 and EC2 guarantee that the polarization states at different frequencies undergo a differential rotation in each section, which is why the background autocorrelation level converges more rapidly. On the other hand, it reduces the convergence to the Maxwellian pdf for polarization rotators, since in this case the polarization rotation is restricted to the XY plane. Without the splice, each section adds a constant amount to the autocorrelation background level. This constant level receives a frequency-dependent rotation in the next section. Thus, the last section plays a large role in determining the background autocorrelation level. Hence, the design ED in which the section lengths decrease yields a very low autocorrelation background level although σ_d and σ_m are fairly large due to the large variation of the section lengths.

It is our view that a 15-section emulator with rotatable sections represents a good design compromise among the two theoretical design criteria that we have proposed as well as ease of implementation. However, additional studies are being carried out in order to develop a technique that allows for the exploration of the performance of these emulators for rare events with large DGD or large frequency derivatives of the polarization dispersion vector, because they are the main cause of outage in optical systems due to PMD.

VII. CONCLUSION

In this paper, we have investigated analytically, numerically, and experimentally the properties of PMD emulators, and we have proposed and examined several different emulator designs.

We began by investigating the properties of emulators with fixed orientations between sections of polarization-maintaining fiber. We found that very large bandwidths—much larger than are currently in use in communications systems—are required in order to obtain a Maxwellian distribution of the DGD over the frequency bandwidth. We also found that splicing the sections at 45° rather than randomly leads to a more rapid convergence. Next, we investigated emulators in which the splicing angle between sections can be changed so that ensembles can be studied. Because the polarization states of communication fibers are constantly changing in the real world, the ability to control the mode coupling is an important property for emulators to possess. We studied emulators with scramblers between the sections that allow the polarization state to be uniformly scattered, and we studied emulators in which the sections rotate relative to one another. In both cases, we were able to derive analytical expressions for the pdf of the DGD, although these expressions grow more complicated as the number of sections increases. We compared these expressions to numerical simulations, and, in the case of rotatable sections, to experiments, and have shown excellent agreement.

Finally, we proposed two criteria for judging the effectiveness of emulators and investigated a number of designs. In general, we found a tradeoff between rapid convergence to a Maxwellian pdf for the DGD as the number of sections increased and rapid convergence to a low background autocorrelation level. We found that emulators with 15 sections appear to be adequate, although further systems studies are clearly required. By contrast, emulators with three sections appear to be clearly inadequate.

APPENDIX

In order to derive the pdf for the DGD between the principal states of polarization in emulators with uniform rotation between the sections, we start from (7), which we rewrite in the form

$$Z^2 = \mathcal{G}(X,Y) = a^2 + Y^2 - 2aYX \tag{28}$$

where $Y = \Delta\tau_n$ is the DGD of the first n sections, $X = \cos(\theta)$ is the cosine of the angle between the two polarization dispersion vectors, which are both random variables, $a = |\Delta\boldsymbol{\Omega}|$ is the constant DGD of the $(n+1)$-th section, and $Z = \Delta\tau_{n+1}$ is the resultant DGD whose pdf is unknown.

Because the polarization is completely scrambled, it can be shown [13] that the cosine of the angle between the polarization dispersion vectors is uniformly distributed between -1 and 1. From the pdf of the random variables X and Y, we can obtain the pdf for the random variable Z using an integral relation described for example by Papoulis [14]

$$f_{Z^2}(z^2)dz^2 = \iint_{\mathcal{G}(x,y)\in[z^2,z^2+dz^2]} f_{X,Y}(x,y)\,dx\,dy. \tag{29}$$

From (28), we then obtain

$$dx = \frac{dz}{2ay}. \tag{30}$$

Noting that X and Y are independent and using (30) in (29), we find

$$f_{Z^2}(z^2) = \int_{-\infty}^{+\infty} \frac{f_X(x)f_Y(y)}{2ay}\,dy. \tag{31}$$

Substituting the pdf of X, which is uniformly distributed between $X = -1$ and $X = 1$, into (31), we obtain the limits of integration by solving for Y in (28), setting $X = \pm 1$. Using also the relation between the pdfs of two interdependent random variables, in this case Z and Z^2, we finally obtain

$$f_Z(z) = \frac{z}{2a}\int_{|z-a|}^{z+a} \frac{f_Y(y)}{y}\,dy \tag{32}$$

which is just (16).

The derivation of (23) follows the same procedure, except that, in the first step of the previous development, the random variable $X = \cos(\theta)$ is derived from an uniform distribution of θ between 0 and 2π.

ACKNOWLEDGMENT

The authors wish to thank B. Marks for carefully reviewing the manuscript.

REFERENCES

[1] I. P. Kaminow, "Polarization in optical fibers," *IEEE J. Quantum Electron.*, vol. 17, pp. 15–22, 1981.
[2] C. R. Menyuk, "Application of multiple-length-scale methods to the study of optical fiber transmission," *J. Eng. Math.*, vol. 36, pp. 113–136, 1999.
[3] C. R. Menyuk and P. K. A. Wai, "Polarization evolution and dispersion in fibers with spatially varying birefringence," *J. Opt. Soc. Amer. B*, vol. 11, pp. 1288–1296, 1994.
[4] D. Sandel, M. Yoshida-Dierolf, R. Noé, A. Schopflin, E. Gottwald, and G. Fisher, "Automatic polarization mode dispersion compensation in 40 Gbit/s optical transmission system," *Electron. Lett.*, vol. 34, pp. 2258–2259, Nov. 1998.
[5] R. Noé, D. Sandel, M. Yoshida-Dierolf, S. Hinz, C. Glingener, C. Scheerer, A. Schopflin, and G. Fisher, "Polarization mode dispersion compensation at 20 Gbit/s with fiber-based distributed equalizer," *Electron. Lett.*, vol. 34, pp. 2421–2422, Dec. 1998.
[6] I. T. Lima Jr., R. Khosravani, P. Ebrahimi, E. Ibragimov, A. E. Willner, and C. R. Menyuk, "Polarization mode dispersion emulator," in *Proc. OFC 2000*, 2000, pp. 31–33. ThB4.
[7] R. Khosravani, I. T. Lima Jr., P. Ebrahimi, E. Ibragimov, A. E. Willner, and C. R. Menyuk, "Time and frequency domain characteristics of polarization-mode dispersion emulators," *IEEE Photon. Technol. Lett.*, vol. 13, pp. 127–129, Feb. 2001.
[8] C. D. Poole, J. H. Winters, and J. A. Nagel, "Dynamical equation for polarization dispersion," *Opt. Lett.*, vol. 16, pp. 372–374, 1991.
[9] M. Karlsson and J. Brentel, "Autocorrelation function of the polarization-mode dispersion vector," *Opt. Lett.*, vol. 24, pp. 939–941, 1999.
[10] P. Ciprut, N. Gisin, R. Passy, J. P. Von der Weid, F. Prieto, and C. W. Zimmer, "Second-order polarization mode dispersion: Impact on analog and digital transmissions," *J. Lightwave Technol.*, vol. 16, pp. 757–771, May 1998.
[11] N. Gisin and J. P. Pellaux, "Polarization mode dispersion: Time versus frequency domain," *Opt. Commun.*, vol. 89, pp. 316–323, 1992.
[12] C. D. Poole, N. S. Bergano, R. E. Wagner, and H. J. Schulte, "Polarization dispersion and principal states in a 147 km undersea lightwave cable," *J. Lightwave Technol.*, vol. 7, pp. 1185–1190, Aug. 1989.
[13] G. Poole and D. L. Favin, "Polarization dispersion measurements based on transmission spectra through a polarizer," *J. Lightwave Technol.*, vol. 12, pp. 917–929, June 1994.

[14] A. Papoulis, *Probability, Random Variables, and Stochastic Processes*. New York, NY: McGraw-Hill, 1984.
[15] C. H. Prola Jr., J. A. P. da Silva, A. O. Dal Forno, R. Passy, J. P. von der Weid, and N. Gisin, "PMD emulators and signal distortion in 2.48 Gb/s IM-DD lightwave systems," *IEEE Photon. Technol. Lett.*, vol. 9, pp. 842–844, June 1997.
[16] N. Gisin, R. Passy, P. Blasco, M. O. Van Deventer, R. Distl, H. Gilgen, B. Perny, R. Keys, E. Krause, C. C. Larsen, K. Mörl, J. Pelayo, and J. Vobian, "Definition of polarization mode dispersion and first results of the COST 241 round-robin measurements," *Pure Appl. Opt.*, vol. 4, pp. 511–522, 1995.
[17] D. Marcuse, C. R. Menyuk, and P. K. A. Wai, "Application of the Manakov-PMD equation to studies of signal propagation in optical fibers with randomly varying birefringence," *J. Lightwave Technol.*, vol. 15, pp. 1735–1746, 1997.
[18] A. Djupsjöbacka, "On differential group-delay statistics for polarization-mode dispersion emulators," *J. Lightwave Technol.*, vol. 19, pp. 285–290, Feb. 2001.
[19] M. Karlsson, "Probability density functions of the differential group delay in optical fiber communication systems," *J. Lightwave Technol.*, vol. 19, pp. 324–331, Mar. 2001.

Ivan T. Lima, Jr. (S'96) received the B.S. and M.S. degrees in electrical engineering, in the are of electronics and communications, from the Federal University of Bahia, Bahia, Brazil, and the State University of Campinas, Campinas, Brazil, respectively. He is currently pursuing the Ph.D. degree in photonics at the University of Maryland Baltimore County, Baltimore, under the supervision of Dr. C. R. Menyuk.

His research interests include the polarization effects in optical fiber communication systems.

Mr. Lima is a member of the Optical Society of America (OSA).

Reza Khosravani (S'98–M'00), photograph and biography not available at the time of publication.

Paniz Ebrahimi received the B.S. degree in electrical engineering from Sharif University of Technology, Tehran, Iran, in 1996. She is currently pursuing the Ph.D. degree in electrical engineering at University of Southern California, Los Angeles.

Her research interests include polarization mode dispersion and fiber nonlinearities.

Edem Ibragimov (M'00), photograph and biography not available at the time of publication.

Curtis R. Menyuk (SM'88–F'98) was born March 26, 1954. He received the B.S. and M.S. degrees from the Massachusetts Institute of Technology, Cambridge, in 1976 and the Ph.D. degree from the University of California, Los Angeles, in 1981.

He has worked as a Research Associate at the University of Maryland, College Park, and at Science Applications International Corporation, McLean, VA. In 1986, he became an Associate Professor in the Department of Electrical Engineering at the University of Maryland Baltimore County (UMBC), Baltimore, and he was the founding member of this department. In 1993, he was promoted to Professor. He has been on partial leave from UMBC since 1996. From 1996 to 2001, he worked part-time for the Department of Defense (DoD), codirecting the Optical Networking Program at the DoD Laboratory for Telecommunications Sciences in Adelphi, MD, from 1999 to 2001. In August, 2001, he left DoD and became Chief Scientist at PhotonEx Corporation. For the last 15 years, his primary research area has been theoretical and computational studies of fiber-optic communications. He has authored or coauthored more than 130 archival journal publications as well as numerous other publications and presentations. He has also edited two books. The equations and algorithms that he and his research group at UMBC have developed to model optical fiber transmission systems are used extensively in the telecommunications industry.

Dr. Menyuk is a Fellow of the Optical Society of America (OSA) and a member of the Society for Industrial and Applied Mathematics and the American Physical Society. He is a former UMBC Presidential Research Professor.

Alan Eli Willner (S'87–M'88–SM'93) received the B.A. degree in physics from Yeshiva University, New York, NY, and the Ph.D. degree in electrical engineering from Columbia University, New York, NY.

He was a Postdoctoral Member of the Technical Staff at AT&T Bell Laboratories, Crawford Hill, NJ, and a Member of Technical Staff at Bellcore. He is currently Professor of Electrical Engineering—Systems at the University of Southern California (USC), Los Angeles. He is the Associate Director for the USC Center for Photonics Technology and is an Associate Director for Student Affairs for the National Science Foundation (NSF) Engineering Research Center in Multimedia. He has been involved in many professional activities, including: Vice-President for Technical Affairs for the IEEE Lasers and Electro-Optics Society (LEOS); Elected Member of the Board of Governors for IEEE LEOS; Co-Chair of the Science and Engineering Council of the OSA; Photonics Division Chair of the OSA; General Chair of the IEEE LEOS Annual Meeting; Program Co-Chair of the OSA Annual Meeting; Program Co-Chair of the Conference on Lasers and Electro-Optics (CLEO); General Co-Chair of the OSA Optical Amplifier Conference; General Co-Chair of the IEEE LEOS Topical Meeting on Broadband Optical Networks; Steering Committee and Technical Committee Member of the Conference on Optical Fiber Communications (OFC); and Technical Program Committee Member of the European Conference on Optical Communications. He has served on the following IEEE LEOS awards committees: Quantum Electronics; William Streifer Scientific Achievement; IEEE Fellow; and Distinguished Lecturer. His editorial positions have included: Editor-in-Chief of the JOURNAL OF LIGHTWAVE TECHNOLOGY (JLT); Editor-in-Chief of the IEEE JOURNAL OF SELECTED TOPICS IN QUANTUM ELECTRONICS; Guest Editor for the Special issue of JLT and the IEEE JOURNAL ON SELECTED AREAS IN COMMUNICATIONS on Multiple-Wavelength Technologies and Networks; and Guest Editor for the IEEE JOURNAL OF QUANTUM ELECTRONICS Focus Issue on Ultra-High-Bandwidth Optical Transmissions Systems. He has more than 300 publications, including one book. His research is in the area of optical fiber communication systems, wavelength division multiplexing, optical amplification, optical networks, and optical interconnections.

Dr. Willner is a Fellow of the Optical Society of America (OSA) and was a Fellow of the Semiconductor Research Corporation. He has received the following awards: the NSF Presidential Faculty Fellows Award from the White House; the David and Lucile Packard Foundation Fellowship in Science and Engineering; the NSF National Young Investigator Award; the Fulbright Foundation Senior Scholar Fellowship, the IEEE LEOS Distinguished Lecturer Award; the USC/Northrop Outstanding Junior Engineering Faculty Research Award; the USC/TRW Best Engineering Teacher Award; and the Armstrong Foundation Memorial Prize.